J Korean Med Sci. 2019 Feb 4;34(5):e37
https://doi.org/10.3346/jkms.2019.34.e37
eISSN 1598-6357·pISSN 1011-8934

JKMS

Original Article
Biomedical Engineering

Alendronate-Anionic Clay Nanohybrid for Enhanced Osteogenic Proliferation and Differentiation

Huiyan Piao,[1*] **Myung Hun Kim**,[1*] **Meiling Cui**,[1] **Goeun Choi**,[1,2] and **Jin-Ho Choy**[1]

[1]Department of Chemistry and Nanoscience, Center for Intelligent Nano-Bio Materials, Ewha Womans University, Seoul, Korea
[2]Institute of Tissue Regeneration Engineering, Dankook University, Cheonan, Korea

Received: Nov 14, 2018
Accepted: Dec 13, 2018

Address for Correspondence:
Jin-Ho Choy, PhD
Department of Chemistry and Nanoscience, Center for Intelligent Nano-Bio Materials, Ewha Womans University, Seoul 03760, Korea.
E-mail: jhchoy@ewha.ac.kr

*Huiyan Piao and Myung Hun Kim contributed equally to this work.

ORCID iDs
Huiyan Piao
https://orcid.org/0000-0001-9998-3411
Myung Hun Kim
https://orcid.org/0000-0003-1638-4822
Meiling Cui
https://orcid.org/0000-0002-3758-7963
Goeun Choi
https://orcid.org/0000-0002-5424-8322
Jin-Ho Choy
https://orcid.org/0000-0002-4149-7100

Funding
This work was supported under the framework of international cooperation program managed by National Research Foundation of Korea (No. 2017K2A9A2A10013104).

ABSTRACT

Background: Alendronate (AL), a drug for inhibiting osteoclast-mediated bone-resorption, was intercalated into an inorganic drug delivery nanovehicle, layered double hydroxide (LDH), to form a new nanohybrid, AL-LDH, with 1:1 heterostructure along the crystallographic C-axis. Based on the intercalation reaction strategy, the present AL-LDH drug delivery system (DDS) was realized with an enhanced drug efficacy of AL, which was confirmed by the improved proliferation and osteogenic differentiation of osteoblast-like cells (MG63).
Methods: The AL-LDH nanohybrid was synthesized by conventional ion-exchange reaction and characterized by powder X-ray diffraction (PXRD), high-resolution transmission electron microscopy (HR-TEM), and Fourier transform infrared (FT-IR) spectroscopy. Additionally, in vitro efficacy tests, such as cell proliferation and alkaline phosphatase (ALP) activity, were analyzed.
Results: The AL was successfully intercalated into LDH via ion-exchange reaction, and thus prepared AL-LDH DDS was X-ray single phasic and chemically well defined. The accumulated AL content in MG63 cells treated with the AL-LDH DDS nanoparticles was determined to be 10.6-fold higher than that within those treated with the intact AL after incubation for 1 hour, suggesting that intercellular permeation of AL was facilitated thanks to the hybridization with drug delivery vehicle, LDH. Furthermore, both in vitro proliferation level and ALP activity of MG63 treated with the present hybrid drug, AL-LDH, were found to be much more enhanced than those treated with the intact AL. This is surely due to the fact that LDH could deliver AL drug very efficiently, although LDH itself does not show any effect on proliferation and osteogenic differentiation of MG63 cells.
Conclusion: The present AL-LDH could be considered as a promising DDS for improving efficacy of AL.

Keywords: Drug Delivery System; Inorganic Delivery Vehicle; Layered Double Hydroxide; Alendronate; Osteogenic Proliferation and Differentiation; Drug-Clay Nanohybrid

INTRODUCTION

Understanding intercellular uptake behavior of nanovehicles is an challenging research area of drug delivery, which has attracted great attention for improving therapeutic benefits of various bioactive molecules (drugs, peptides, proteins, and DNA, etc.), particularly those

Disclosure

The authors have no potential conflicts of interest to disclose.

Author Contributions

Conceptualization: Piao H, Kim MH. Formal analysis: Piao H, Kim MH. Cui M, Choi G. Writing - original draft: Piao H, Kim MH. Writing - review & editing: Piao H, Choy JH.

having some weakness such as difficulty and inefficiency crossing the cell membrane due to their enzymatic drug degradation, low circulation stability, and lack of target specificity.[1-3] In the past few decades, many efforts have been made to design various inorganic nanovehicles to induce enhanced cellular uptake behavior based on the surface modification strategy for targeted delivery, low toxicity, and controlled release property.[4,5]

Among various inorganic delivery carriers, layered double hydroxide (LDH) has been suggested as a promising nanovehicle for the encapsulation and intercellular delivery of biological molecules.[6-8] In general, LDH, known as an anionic clay, is represented by a general chemical formula $(M^{2+}_{1-x}M^{3+}_{x}\,[OH]_2)^{x+}(A^{n-})_{x/n}{\cdot}yH_2O$, where M^{2+}, M^{3+}, and A^{n-} are di-, tri-valent metal cations and interlayer anions, respectively.[9] The isomorphic substitutions of M^{2+} with M^{3+} in brucite-like layers give rise to the positive layer charge, and thus anionic species can be encapsulated in between layers of LDH in order to satisfy the charge neutrality condition.[10,11]

High anion exchange capacity (AEC) of LDH offers to intercalate various kinds of negatively charged bioactive molecules into the interlayer space of LDHs via simple co-precipitation or ion-exchange reactions, resulting in novel bio-inorganic nanohybrids.[12,13] And at the same time, the positive surface charge of LDH enables easy approach and adhesion to cell membranes with negative charge inherently by electrostatic interactions without further chemical modifications.[14] Most importantly, it has been already confirmed that LDH nanovehicle with a size of around 100 nm could deliver bioactive molecules very efficiently through its unique cellular uptake mechanism, clathrin-mediated endocytosis.[15,16] As compared to other inorganic nanovehicles, including silica and gold nanoparticles, quantum dots, and carbon nanotubes, LDH was proved to be highly advantageous due to its excellent biocompatibility,[17] high drug loading capacity[18] and pH-responsive property[19] with biodegradability in the cellular cytoplasm[16] and therefore, applicable as an efficient non-viral drug delivery vehicle and also as a reservoir for bioactive or bio-fragile molecules.

Alendronate (AL) itself has been clinically used to treat patients with diseases from osteoclast-mediated bone resorption such as bone metastasis, hypercalcemia of malignancy, post-menopausal osteoporosis and Paget's disease[20,21] because it impedes bone resorption by selective uptake and absorption to divalent ions in bone due to its strong chelating molecular configuration with di-phosphates (P–O–P and P–C–P).[22] Moreover, it has been proved to not only inhibit osteoclastic bone resorption but also induce mineralization of newly formed bone by osteoblasts.[23-25] However, AL has its intrinsic adverse effect such as low intracellular permeability, which in turn results in low drug efficacy.[26] It is, therefore, highly required to find an appropriate delivery vehicle for AL to overcome such a drawback. As appeared in the literature,[27] there was only one trial related to the intercalation reaction of AL into LDH vehicle, however, all the samples were neither X-ray single phasic nor chemically defined, due to the fact that the intercalation reaction could not reach to an equilibrium.[27] In the present study, an attempt has been made to enhance the cellular uptake efficacy of AL, an anti-resorptive and bone-remodeling drug, by encapsulating it into the drug delivery vehicle (LDH), to form a drug-LDH nanohybrid (i.e., AL-LDH) with two-dimensional heterostructure. In this respect, we intended to prepare X-ray single phasic AL-LDH considering various parameters in the reaction solution such as pH, concentration of AL, and AEC of LDH. To the best of our knowledge, this is the first study to examine the cellular uptake efficacy of single phasic AL-LDH structurally and chemically well-defined on the proliferation and osteogenic differentiation of human osteoblast-like cells (MG63).

https://doi.org/10.3346/jkms.2019.34.e37

METHODS

Materials

All chemicals of magnesium nitrate hexahydrate ($Mg[NO_3]_2 \cdot 6H_2O$), zinc nitrate hexahydrate ($Zn[NO_3]_2 \cdot 6H_2O$), aluminum nitrate nonahydrate ($Al[NO_3]_3 \cdot 9H_2O$), AL in sodium trihydrate form ($C_4H_{12}NaNO_7P_2 \cdot 3H_2O$), sodium hydroxide (NaOH), sodium carbonate (Na_2CO_3), fluorescein 5'-isothiocyanate (FITC), ferric chloride hexahydrate ($FeCl_3 \cdot 6H_2O$) and β-glycerophosphate, dexamethasone, and L-ascorbic acid were purchased from Sigma (St. Louis, MO, USA). Perchloric acid ($HClO_4$) was obtained from Junsei (Tokyo, Japan). Dulbecco's modified Eagle's essential medium (DMEM), 0.25% Trypsin-EDTA (1X) and Dulbecco's phosphate-buffered saline (DPBS) were obtained from Gibco (Grand Island, NY, USA).

Preparation of the pristine LDHs and nanohybrids

10 mmol $Mg(NO_3)_2 \cdot 6H_2O$ and 5 mmol $Al(NO_3)_3 \cdot 9H_2O$ were dissolved in 100 mL decarbonated water. For nitrate and carbonate forms of Mg_2Al-LDH (abbreviated as $Mg_2Al\_NO_3$ LDH and $Mg_2Al\_CO_3$ LDH, respectively), each of the mixed metal solutions was titrated with 0.5 M NaOH solution and a mixture of 0.5 M NaOH containing basic Na_2CO_3 (50 mM), respectively, to adjust the pH 10.0, which was then aged for 12 hours. The resulting white precipitate was collected by centrifugation and washed with decarbonated water to remove soluble unreacted ions. A dry powder of $Mg_2Al\_NO_3$ LDH and $Mg_2Al\_CO_3$ LDH was obtained by freeze-drying. With the same method, nitrate and carbonate type of Zn_2Al-LDHs coprecipitated at pH 8.0 (abbreviated as $Zn_2Al\_NO_3$ LDH and $Zn_2Al\_CO_3$ LDH, respectively) were prepared by using $Zn(NO_3)_2 \cdot 6H_2O$ instead of $Mg(NO_3)_2 \cdot 6H_2O$.

And then attempts have been made to prepare AL intercalated LDH nanohybrids based on the ion-exchange reaction. At first, 0.05 M solution of AL in 100 mL of decarbonated water was adjusted to pH 8.0 with 0.5 M NaOH solution in order to dissociate the protons in AL. Each suspension of $Mg_2Al\_NO_3$ LDH, $Mg_2Al\_CO_3$ LDH, or $Zn_2Al\_NO_3$ LDH was then intermixed with this AL solution and the final solution pH was maintained at 10.9 for 24 hours. Each of the resulting precipitates was separated by centrifugation and washed thoroughly with decarbonated water, and then freeze-dried to yield powdery product, AL-$Mg_2Al\_NO_3$ LDH, AL-$Mg_2Al\_CO_3$ LDH, and AL-$Zn_2Al\_NO_3$ LDH, respectively.

For FITC adsorbed $Zn_2Al\_CO_3$ LDH (FITC-LDH-CO_3), the equal volumes of FITC (5 mg/mL) and $Zn_2Al\_CO_3$ LDH (5 mg/mL) were mixed together, followed by stirring for 12 hours. The resulting precipitate was washed 5 times with DI water to remove the excess FITC and freeze-dried.

Characterizations

Powder X-ray diffraction (PXRD) patterns were measured with a diffractometer (D/MAXRINT 2200-Ultima, Rigaku, Japan) equipped with Ni-filtered Cu-Kα radiation (λ = 1.5418 Å). The high-resolution transmission electron microscopy (HR-TEM) image of AL-LDH was obtained with a JEM-2100F (JEOL, Tokyo, Japan), which was operated at an accelerating voltage of 200 kV. Fourier transform infrared (FT-IR) spectra were measured with a JASCO 6100 spectrophotometer (JASCO, Tokyo, Japan) with a potassium bromide disk pellet method. Field emission scanning electron microscopy (FE-SEM) images were measured with a JSM-6700F (JEOL). The size distribution and surface charge were recorded using Nano ZS (Malvern, UK).

https://doi.org/10.3346/jkms.2019.34.e37

The $FeCl_3$ standard solution (5 mM) in a 2 M $HClO_4$ was used to measure the contents of AL in the AL-$Zn_2Al\_NO_3$ LDH (from here abbreviated as AL-LDH). Five different concentrations of AL, ranging from 0.025 to 2.5 mM, were dissolved in 2 M $HClO_4$. A mixture of AL and $FeCl_3$ standard solution (1:1, v./v.) was measured by UV-Vis spectrophotometer (Lambda 35; PerkinElmer, Waltham, MA, USA) to prepare a calibration curve for AL.[28] The AL-LDH particles were dissolved in 2 M $HClO_4$ solution and filtered with Nylon syringe filter (0.45 μm pore; Merck Millipore, Burlington, MA, USA). Then, the dissolved AL from AL-LDH was mixed with the $FeCl_3$ standard solution (1:1, v./v.). The resulting mixtures were measured by UV-Vis spectrophotometer. Inductively coupled plasma-atomic emission spectrometry (ICP-AES) analyses with Optima-4300 DV (PerkinElmer) and elemental CHNS analyses with EA1110 (CE instrument, Milan, Italy) were further carried out in order to confirm chemical compositions of the $Zn_2Al\_NO_3$ and AL-LDH.

In vitro drug release test

To examine in vitro drug release profile, the AL-LDH particles were suspended in 900 mL of pH 7.4 phosphate-buffered saline (PBS) at 37°C and continuously stirred at 125 rpm using a dissolution apparatus 2 (paddle type, Vision® G2 Elite 8TM Dissolution Tester, Hanson, MA, USA). At a scheduled time for 100 days, 3 mL of the medium was collected and the same amount of fresh PBS was added back. The sampled medium was filtered with Nylon syringe filter (0.45 μm pore, Merck Millipore), which was added to the $FeCl_3$ standard solution to quantitatively measure the released amount of AL out of AL-LDH using UV-Vis spectrophotometer. At least three batches of samples were tested for statistics.

In vitro study

MG63 cells (Korean Cell Line Bank) were grown in DMEM medium supplemented with 10% heat inactivated fetal bovine serum, 100 units/mL penicillin, and 100 μg/mL streptomycin under a 5% CO_2 atmosphere with 95% humidity at 37°C. When the cells grew up to 80%–90% confluence, they were isolated from cell culture dishes by trypsinization and washed with 10 mM DPBS.

Quantification of accumulated AL in MG63 cells

MG63 cells seeded on a 60 mm culture dish at 2.0×10^6 cells per well were treated with intact AL or AL-LDH containing at the equivalent concentration of AL (50 μg/mL). After the given incubation time for 1, 2, 4, 6, 12, and 24 hours, the cells were washed two times with DPBS, harvested by trypsin-EDTA treatment, and separated by centrifugation. After the precipitated pellets were washed twice with DPBS, 5 mL of cell lysis buffer (20 mM Tris-HCl, pH 7.5, 1% Triton X-100, 150 mM NaCl, and 1 mM EDTA) was added and the pellets were incubated on ice for 20 minutes followed by ultrasonication (Sonics & Materials Inc., Newtown, CT, USA) for 20 seconds. After centrifuging the crude cell lysates at 10,000 rpm for 5 minutes, 10 mL acetonitrile (DAEJUNG, Siheung, Korea) was added to the cell supernatants, and the resulting mixture was vigorously vortexed to precipitate proteins. After further centrifugation of the mixture at 10,000 rpm for 3 minutes, 20 mL chloroform (DAEJUNG) was added to the supernatant to remove lipids, which was then collected by centrifugation at 2,000 rpm for 10 minutes. The final supernatant was added to the $FeCl_3$ standard solution to measure the concentration of AL using UV-Vis spectrophotometer. Each experiment was repeated at least three times.

Confocal laser scanning microscopy (CLSM) study

For CLSM measurements, MG63 cells in 2 mL of DMEM medium (2.0×10^6 cells per well) were seeded in Coverglass bottom dish (SPL Lifesciences Co., Ltd., Pocheon, Korea) and

https://doi.org/10.3346/jkms.2019.34.e37

incubated at 37°C and 5% CO_2 for 24 hours. Then, the medium in the well was replaced by the FITC-LDH-CO_3 suspension (20 μg/mL) in fresh medium and incubated under the same condition. A control experiment was also performed with intact FITC (20 μg/mL) and the centrifugal supernatant of the FITC-LDH-CO_3 suspended in the cell medium under the same conditions. After incubation for 1 hour, the cells were washed three times with DPBS and fresh cell medium were then added to the plates. For the staining of nucleus, 140 μL of NucBlue (Live Cell Stain ReadyProbes® reagent; Thermo Fisher Scientific, Waltham, MA, USA) was added and incubated for additional 20 minutes at 25°C. The stained cells were imaged under a confocal laser scanning microscope (Leica TCS SP8 STED CW; Leica Microsystems Inc., Buffalo Grove, IL, USA) equipped with both DAPI filter (Ex. 420 nm/Em. 460 nm) and FITC filter (Ex. 495 nm/Em. 520 nm). The obtained images were processed using Leica LASAF software.

Proliferation study

The MG63 cells were seeded onto 96-well plates at 2×10^4 cells per well and incubated at 37°C under a 5% CO_2 atmosphere for 24 hours. Then, the cell medium in each well was completely substituted with osteogenic medium (2 mM L-glutamine, 10 mM β-glycerophosphate, and 50 ng/mL L-ascorbic added to cell media) containing pristine LDH ($Zn_2Al\_NO_3$ LDH), intact AL, or AL-LDH, and the cells were cultured for 2, 3, or 4 days. At every predetermined time, the cells were washed with DPBS, and the cell proliferation was assessed with CCK-8, following the manufacturer's instruction.[29] Briefly, 100 μL CCK-8 solution was added into each well and cultured for additional 3 hours and then the optical density of each well was measured at 450 nm on a microplate reader (Multiskan FC, Thermo Fisher Scientific), and expressed in percentage based on the optical density of negative control (only osteogenic medium was treated to the cells). The assay was performed at least three times for statistics.

Alkaline phosphatase (ALP) activity

MG63 cells were cultured in 6-well plates at 1.5×10^5 cells per well and incubated overnight at 37°C under a 5% CO_2 atmosphere for 24 hours. The cell medium in each well of the plate was completely substituted with the osteogenic medium containing pristine LDH ($Zn_2Al\_NO_3$ LDH), intact AL, or AL-LDH and treated under the same conditions described above. At a given time, the adherent cells were scraped off and suspended in 3 mL of osteogenic medium, which was shaken at 4°C for 10 minutes and centrifuged at 2,500 rpm for 10 minutes. The supernatant (50 μL) was then transferred to 96-well plate and the same volume of PNPP solution was added.[23] The total amounts of released enzyme from the cells were spectrophotometrically measured by a microplate reader (Multiskan FC, Thermo Fisher Scientific) at 405 nm. At least three times were tested for each sample type.

Statistical analysis

All data for in vitro cell proliferation and ALP activity was applied in one-way ANOVA with $\alpha = 0.05$ followed by pairwise comparisons using a Tukey's post hoc test (Prism, version 5.01; GraphPad, San Diego, CA, USA). $P < 0.05$ was considered statistically significant.

RESULTS

PXRD analysis

In the previous work,[27] an attempt was made to intercalate AL into LDH, but failed to prepare chemically well-defined AL-LDH nanohybrid. According to the PXRD analysis, no X-ray

https://doi.org/10.3346/jkms.2019.34.e37

single phasic AL-LDH was synthesized due to the formation of thermodynamically stable carbonate ion intercalated LDH. Thus, we intended to find out synthetic conditions for the X-ray single phasic AL-LDH by taking account AL concentrations in a reaction solution and the pH of the solution as well. According to the calculated molar fraction of AL depending on pH (**Supplementary Fig. 1**), AL may exist in the forms of AL^{2-} = 0.49, AL^{3-} = 0.49, and AL^{4-} = 0.02 at pH 10.9, in which primary amine group in AL could be considered to be almost deprotonated. Thus, we set the pH of solution at 10.9 in order for the intercalative ion-exchange reaction of AL into LDH not to be disturbed by protonated primary amine in AL.

A 2.5-fold excess amount of AL was reacted with the carbonate type of Mg_2Al-LDH ($Mg_2Al\_CO_3$ LDH) and the nitrate type ($Mg_2Al\_NO_3$ LDH), respectively, at pH 10.9. As shown in **Supplementary Fig. 2A and B**, the AL molecules were not successfully intercalated into both LDHs. The XRD patterns of $Mg_2Al\_CO_3$ LDH remained unchanged with respect to the reaction time, indicating that no intercalation of AL into LDH occurred. In the case of $Mg_2Al\_NO_3$ LDH, however, the intercalation reaction could be observed, but resulted in the formation of two phases, AL intercalated LDH and unreacted $Mg_2Al\_NO_3$ LDH, within 24 hours. On the other hand, a single phasic AL-LDH was realized, when the nitrate type of $Zn_2Al\_NO_3$ LDH was intercalated as shown in **Supplementary Fig. 2C**. Though the AL intercalated LDH was coexisted with the unreacted within the reaction time of 8 hours, the intercalation reaction of AL into the $Zn_2Al\_NO_3$ LDH was reached to an equilibrium beyond 12 hours, where well-ordered (*00l*) reflections could be observed for AL-$Zn_2Al\_NO_3$ LDH (abbreviated as AL-LDH).

As shown in **Fig. 1A**, the basal spacing was expanded to 11.3 Å from 8.7 Å (that of $Zn_2Al\_NO_3$ LDH) upon intercalation of AL. The gallery height of AL-LDH was estimated to be 6.5 Å (11.3 Å – 4.8 Å [the thickness of LDH single layer]), which was smaller than the molecular dimension of AL as shown in **Supplementary Fig. 3A and B**. It is, therefore, expected that AL molecules were likely to be stabilized with a monolayer arrangement as shown in **Supplementary Fig. 3C**.

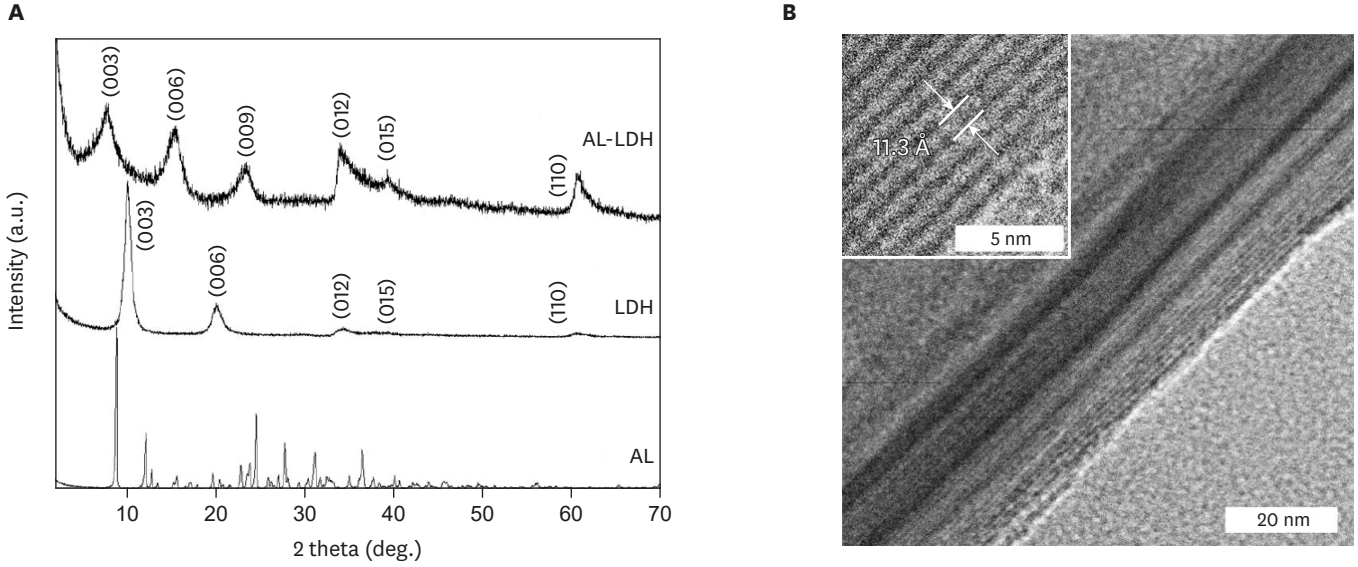

Fig. 1. Crystal structures. (**A**) PXRD patterns of intact AL, pristine LDH, and AL-LDH. (**B**) HR-TEM image of AL-LDH with inset of higher magnification.
PXRD = powder X-ray diffraction, AL = alendronate, LDH = layered double hydroxide, HR-TEM = high-resolution transmission electron microscopy.

https://doi.org/10.3346/jkms.2019.34.e37

To confirm this configuration, we investigated the steric limitation between the intercalated AL molecules and positively charged sites of LDH layers, which can be explained by the equivalent area (A_e, area per positive unit charge of LDH) and the demanded area (A_c, area per negative unit charge for intercalated single molecule). A_e of the layered host lattice can be calculated from the following equation: $A_e = a \cdot b \cdot \sin\gamma/\xi$, where a and b are lattice parameters and ξ is the layer charge per formula unit. Based on the lattice parameters of AL-LDH (a = b = 3.07 Å, c = 33.78 Å, $\gamma = 120^\circ$ and $\xi = 1/3e^-$), A_e of LDH could be calculated as 24.5 $Å^2$, slightly larger than the demanded area (A_c) of AL (24.0 $Å^2$). In the range of $A_e > A_c$, the guest molecules could be incorporated between the LDH layers with parallel monolayer orientation along the ab plane of LDH.

In order to gain further insight in the arrangement of intercalated AL molecules in the interlayer space of LDH, we compared the relative intensity (I_{rel}) of the observed X-ray intensity (I_{obs}) to that of the calculated one (I_{cal}) from the structural models of AL-LDH (**Supplementary Fig. 4A-C**). The structure factor (F[*00l*]) of the each structural model was obtained from the atomic scattering factor for each atom in the unit cell (f_i) and the position of atoms (z_i) along c-axis based on the following equation, $F(00l) = \sum_{i=0}^{N} f_i \cos(2\pi l z_i)$.[30] The integrated intensity of (*00l*) diffraction peak (I[*00l*]) was proportional to the square of F(*00l*) and to Lorentz-Polarization factor ($LP[\theta] = [1+\cos^2 2\theta]/[\cos \cdot \sin^2\theta]$).

Taking into account of steric limitation between the intercalated AL molecules and the positively charged sites of LDH layer, the basal spacing of AL-LDH, and the molecular dimension of AL, three structural models of AL-LDH could be suggested as follows; 1) two phosphate groups of AL molecule were electrostatically interacted with up and down sides of LDH layers as shown in **Supplementary Fig. 4A**, and **2**) two phosphate groups of AL molecule were electrostatically interacted with only one side (up or down side) of LDH layer as shown in **Supplementary Fig. 4B and C**. Although it was not easy to refine the interlayer structure of AL-LDH due to the limited number of (*00l*) diffractions, the interlayer structure of AL-LDH in **Supplementary Fig. 4C** would be highly probable among those three models: the I_{cal} values from the model were close to the I_{obs} values, as shown in **Supplementary Fig. 4D**.

HR-TEM study

From the cross-sectional HR-TEM image of AL-LDH as shown in **Fig. 1B**, well-ordered 2D structure of AL-LDH could be confirmed. The distance between the lattice fringes along the crystallographic C-axis was observed to be approximately 11.3 Å, which was in excellent agreement with the d_{00l} value obtained from the PXRD pattern.

FT-IR analysis

The FT-IR spectrum of AL-LDH was compared to those of intact AL and pristine LDH ($Zn_2Al\_NO_3$ LDH) (**Fig. 2**). For intact AL, the characteristic infrared vibration bands, such as O-H of phosphate (3,490 cm^{-1}), C-H (2,965 cm^{-1}), N-H (1,545 cm^{-1}), C-O-C (1,119 cm^{-1}), P = O (1,056 cm^{-1}), and P-O (960 cm^{-1}), were clearly observed.[31,32] For the pristine LDH, the broad absorption bands at 3,451 and 1,642 cm^{-1} were assigned as O-H stretching vibration from the hydroxide layer and the interlayer water in LDH, respectively. The absorption bands observed in the low frequency region below 800 cm^{-1} were attributed to the lattice vibration modes from M-O and M-O-M (M: metals, such as Zn and Al) bonds. All the characteristic bands from intact AL and pristine LDH were overlapped within those of AL-LDH. Particularly, the nitrate absorption peak at 1,382 cm^{-1} found in pristine LDH was disappeared in AL-LDH, indicating that the interlayer nitrate ions were completely replaced with negatively charged

https://doi.org/10.3346/jkms.2019.34.e37

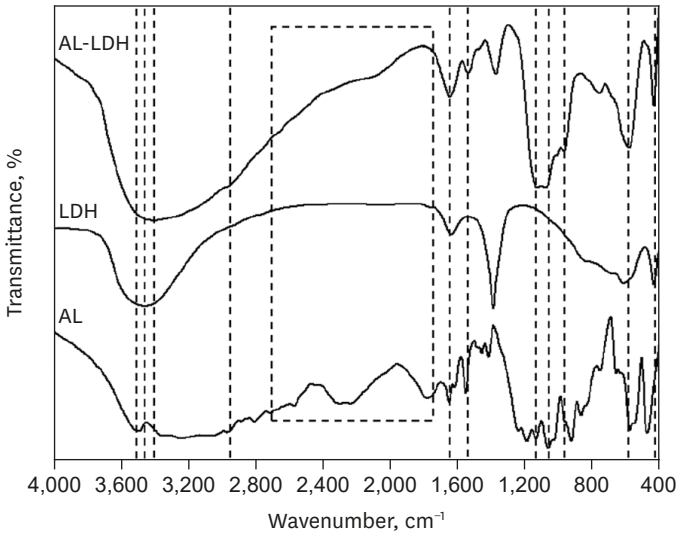

Fig. 2. FT-IR spectra of intact AL, pristine LDH, and AL-LDH.
FT-IR = Fourier transform infrared, AL = alendronate, LDH = layered double hydroxide.

AL molecules through the intercalative ion-exchange reaction. The broad peak between 1,800 and 2,700 cm^{-1} corresponding to the O-H stretching absorption in the O = P-OH group of AL,[33] was disappeared in AL-LDH due to the deprotonation of OH groups, which were electrostatically interacted with the LDH layers.

Particle size and surface charge studies

According to the field emission scanning electron microscopy (FE-SEM) images (**Fig. 3A and B**), the plate-like LDH particles with an average size of around 120 nm were not that changed upon intercalation of AL to form AL-LDH, indicating that the intercalation reaction proceeded without any structural reconstruction, but went on topotactically. According to the dynamic light scattering (DLS) analysis (**Fig. 3C**), the particle sizes were measured to be 118 ± 13 nm and 120 ± 11 nm for the pristine LDH and AL-LDH, respectively, which were in good agreement with the FE-SEM data. Furthermore, as shown in **Fig. 3D**, the surface charge of pristine LDH was determined to be 35.1 ± 0.1 mV, but such a distinctive positive surface charge became reduced to 0.3 ± 0.15 mV upon intercalation of AL, due to the strong electrostatic interaction between the negatively charged AL and positively charged LDH layer.

UV-Vis spectroscopy

The AL content in the AL-LDH was determined through UV-Vis spectrophotometric analysis using $FeCl_3$ standard solution. Since AL does not contain an appreciable chromophore, AL was complexed with Fe^{3+} ions under an acidic condition of 2 M $HClO_4$, in which the hydrolysis of Fe^{3+} ions could be avoided.[32] The absorption spectra of base line (2 M $HClO_4$), intact AL only, AL-LDH only, Fe^{3+} standard, and Fe^{3+}–AL complexes were recorded in the wavelength range of 200–400 nm (**Supplementary Fig. 5A**). As expected, no UV absorbance appeared for intact AL and AL-LDH, but the absorption peaks with λ_{max} for the Fe^{3+} standard and Fe^{3+}–AL complexes were clearly observed. The absorbances of Fe^{3+}–AL complexes were read at 300 nm depending on the concentrations of AL in order to obtain a calibration curve of AL (**Supplementary Fig. 5B**).

On the basis of calibration curve, the AL content in AL-LDH was determined to be 26.5%, which was in excellent agreement with the theoretical one (26.3%). Briefly, the latter was

https://doi.org/10.3346/jkms.2019.34.e37

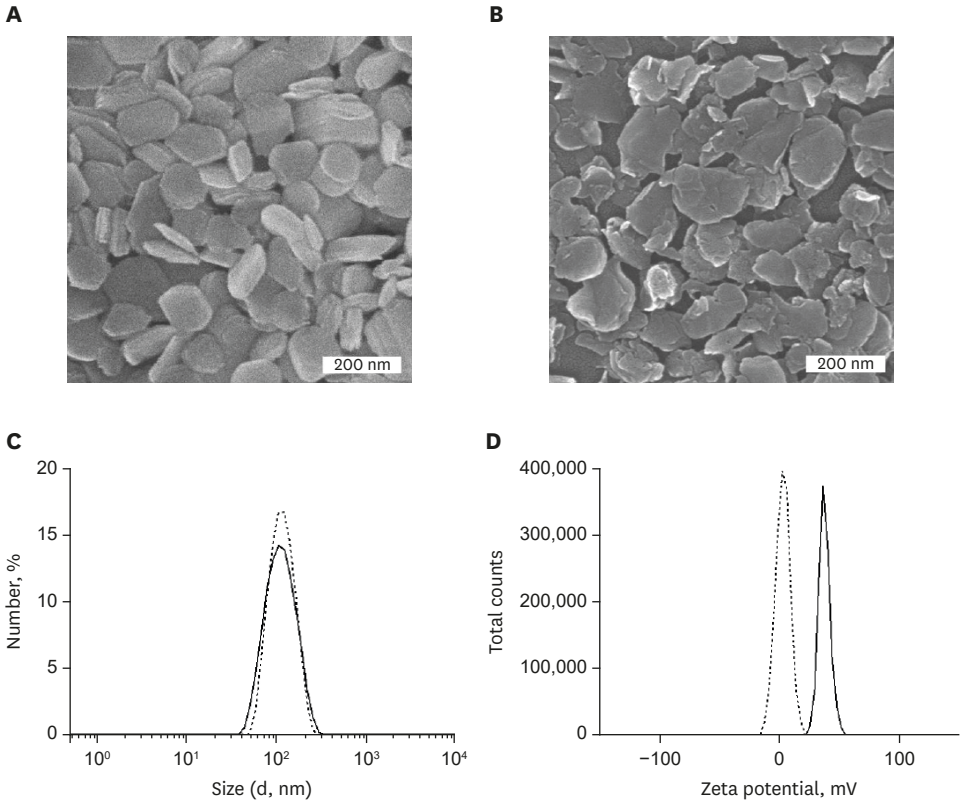

Fig. 3. Particle size and surface charge analyses. FE-SEM images of (**A**) pristine LDH and (**B**) AL-LDH. (**C**) Particle size distributions and (**D**) zeta potentials of pristine LDH (solid line) and AL-LDH (dashed line), respectively.
FE-SEM = field emission scanning electron microscopy, LDH = layered double hydroxide, AL = alendronate.

determined on the basis of the net charge of AL (−2.54) calculated by its mole fractions, AL^{2-} = 0.49 and AL^{3-} = 0.49, at pH = 10.9, which was also the synthetic condition of AL-LDH. According to the ICP-AES, and elemental CHN analysis, the chemical compositions for the pristine LDH and its AL intercalated were determined as $Zn_{0.67}Al_{0.33}(OH)_2(NO_3)_{0.33}\cdot 0.32H_2O$ and $Zn_{0.68}Al_{0.32}(OH)_2AL_{0.13}\cdot 0.28H_2O$, respectively.

In vitro release test

According to the in vitro cumulative AL release profile from AL-LDH as shown in **Fig. 4**, the AL molecules seemed to be hardly deintercalated under the condition of the PBS solution pH of 7.4 at 37°C. At the initial stage, prevalent anions in PBS, such as anionic forms of phosphate and chloride, facilitated the desorption of AL molecules on the external surface of the AL-LDH nanoparticles, resulting in the initial burst (5%) of AL. After 2 days, however, another 4.5% of AL in the interlayer space of LDH was very slowly released out until 100 days. More than 90% of AL molecules were thermodynamically stabilized in the 2D lattice, and eventually remained as the AL-LDH hybrid, due to the strong electrostatic interaction between deprotonated AL molecules and positively charged LDH lattice.

As described in the structural model of AL-LDH (**Supplementary Fig. 6A**), the deprotonated phosphate group of AL bound to only one side of LDH layer by strong electrostatic interaction, resulting in the controlled release of AL from AL-LDH. One other possible explanation for that might be the zipping effect of layered edges bonded with small anions present in the PBS solution, and therefore, AL molecules can be locked up there

https://doi.org/10.3346/jkms.2019.34.e37

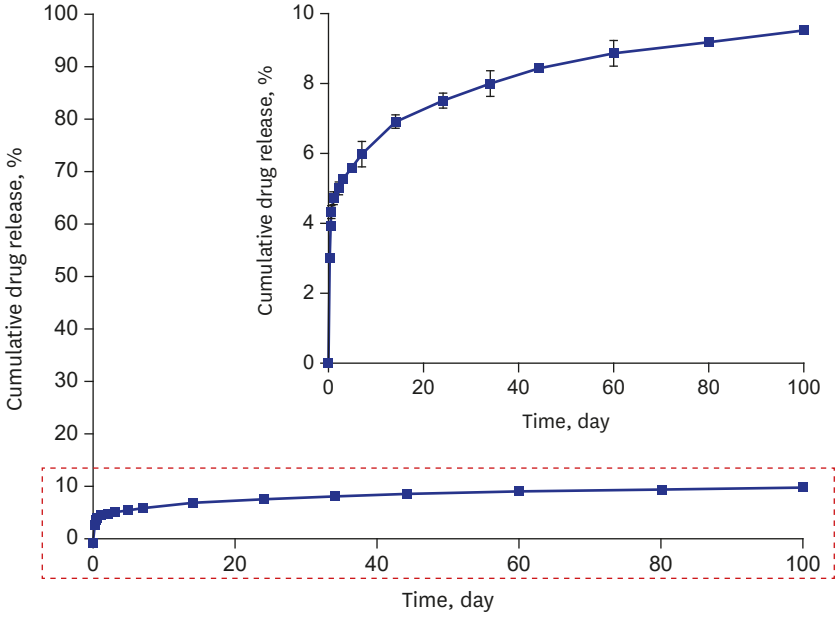

Fig. 4. In vitro cumulative AL release profile of AL-LDH in pH 7.4 PBS.
AL = alendronate, LDH = layered double hydroxide, PBS = phosphate-buffered saline.

in the interlayer space of LDH, giving rise to the retarded out-diffusion from AL-LDH (**Supplementary Fig. 6B**).[34]

In order to rationalize the release behavior of AL from AL-LDH depending on the above assumptions, the observed release profile of AL-LDH was fitted to four kinetic models as shown in **Supplementary Fig. 7** and the obtained rate constants (k_d) and r^2 values were summarized in **Supplementary Table 1**. The first-order kinetic model, describing dissolution phenomena, was not an option to be considered due to the poor r^2 value (0.66), indicating that the release of AL from AL-LDH does not mainly depend on the dissolution determined process.[34] In contrast, the parabolic diffusion model, which is a modified Freundlich model, and Elovich one were well fitted to the observed release profile of AL with reliable r^2 values of more than 0.95. It is, therefore, suggested that the AL release process is a kind of diffusion-controlled process or heterogeneous diffusion processes.[34]

Cellular uptake studies

In order to verify efficient cellular uptake behavior of LDH, we quantified the accumulated concentration of AL in MG63 cells with respect to incubation time. As shown in **Fig. 5**, MG63 cells treated with the AL-LDH nanoparticles exhibited 10.6 times higher intracellular accumulation of AL than those treated with intact AL at the 1hour incubation time, indicating that LDH, as a delivery vehicle, could facilitate permeation of AL into MG63 cells. Such an improved uptake efficacy of AL with LDH was greatly superior to that with other AL delivery systems, such as chitosan coated polyethylene oxide microsphere and chitosan coated liposome, which showed only 3-fold and 2-fold increases, respectively.[29] The concentration of AL in MG63 cells treated with AL-LDH was rapidly increased up to 11.16 μg/mL within 1 hour, but gradually decreased with time. Throughout all incubation periods, AL-LDH exhibited much higher intracellular uptake efficacy than intact AL. As expected, intact AL cannot easily be permeated inside the cells due to repulsive interaction between the negatively charged cell membrane and anionic AL molecules. On the other hand, the positive layer charge of

https://doi.org/10.3346/jkms.2019.34.e37

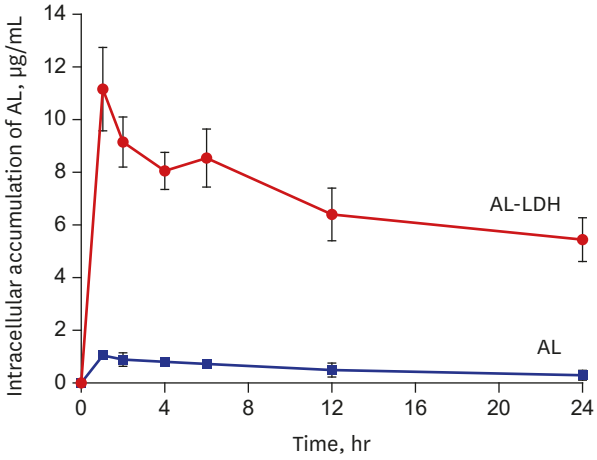

Fig. 5. Cellular accumulation of AL molecules in MG63 cells treated with either intact AL or AL-LDH.
AL = alendronate, LDH = layered double hydroxide.

LDH became mostly neutralized upon intercalation of anionic AL to form AL-LDH with a slightly positive charge, which can electrostatically interact with the cellular membranes, leading to favorable cellular uptake based on clathrin-mediated endocytosis.[15] It is, therefore, concluded that LDH could play a role as an efficient drug delivery carrier.

To trace intercellular pathway of LDH visually, the LDH-CO_3 nanoparticles were conjugated with a dye, FITC, to form FITC-LDH-CO_3, which was then incubated in MG63 cell culture line and its permeation behaviour was studied by the CLSM as shown in **Supplementary Fig. 8** and **Supplementary Fig. 9**. The green fluorescence was observed throughout the cytoplasm of MG63 cells cultured with 20 μg/mL of FITC-LDH-CO_3 for 1 hour (**Supplementary Fig. 10A**). On the contrary, the green fluorescence was not detected within cells in the control experiments (**Supplementary Fig. 10B and C**), which was carried out with the centrifugal supernatant of FITC-LDH-CO_3 and intact FITC solution, respectively. And it became clear that the green fluorescence within cells was not from free FITC, but from the uptake of the FITC-LDH-CO_3 nanoparticles

In vitro cell proliferation and ALP activity

To assess the drug-carrier efficacy, we also investigated the effects of AL-LDH on the cell proliferation and osteogenic differentiation in the MG63 cell culture line, which was compared to those of intact AL and pristine LDH. And the cells treated with the osteogenic medium only were employed as the control.

In vitro proliferation level of MG63 cells was investigated on the basis of colorimetric CCK-8 assay, which has been widely used for determining the cell viability in terms of cell proliferation and cytotoxicity.[29] As shown in **Supplementary Fig. 11**, both intact AL and AL-LDH showed higher cell proliferation in all concentrations of AL during the whole tested period than the pristine LDH. One thing to note here was that the cells incubated with AL-LDH gave rise to an enhanced cell proliferation compared to intact AL in all conditions. As shown in **Fig. 6**, the highest cell proliferation was observed at the concentration of 1×10^{-8} M AL for both intact AL and AL-LDH, which were 29.8% and 59.8%, respectively, above the negative control value. However, no increase in cell proliferation could be observed for the pristine LDH. The cell proliferation for all the samples tested was either increased or maintained even after 2 day incubation, indicating that AL-LDH and the pristine LDH were not cytotoxic, which could be also supported by our previous studies.[35,36]

https://doi.org/10.3346/jkms.2019.34.e37

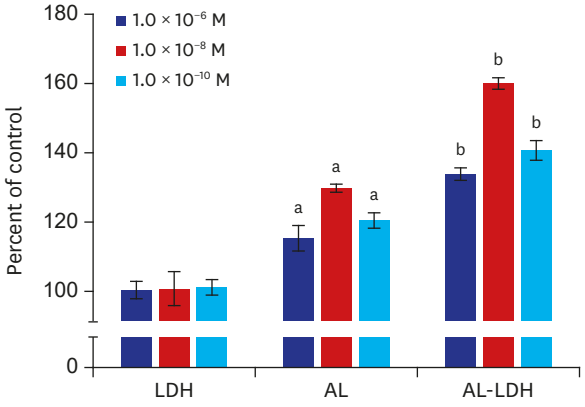

Fig. 6. In vitro proliferation of MG63 cells treated with osteogenic media containing different concentrations of pristine LDH, intact AL, and AL-LDH for 3 days. For each sample type, at least three experiments were performed for statistics.
LDH = layered double hydroxide, AL = alendronate.
[a]Intact AL was statistically significantly different from pristine LDH ($P < 0.05$); [b]AL-LDH was statistically significantly different from both pristine LDH and intact AL ($P < 0.05$).

The efficacy of cell differentiation was also evaluated for AL-LDH together with intact AL in terms of ALP activity, which has been widely used as a marker for early differentiation of osteoblast-like cells to demonstrate improved osteogenic activity.[23] As can be seen in **Supplementary Fig. 12**, both intact AL and AL-LDH showed higher ALP activities of MG63 cells than pristine. In particular, the ALP activities on the day 3 and 4 were significantly increased for the cells treated with intact AL only at the concentration of 10^{-8} M AL. On the other hand, AL-LDH exhibited statistically significant difference in ALP activity at any given concentrations of AL during whole tested periods as compared to the pristine LDH and the negative control ($P < 0.05$). As shown in **Fig. 7**, the highest increases in ALP activity of MG63 cells relative to that of negative control group were 12.4% and 29.1% at the concentration of 10^{-8} M AL of intact AL and AL-LDH, respectively. Additionally, ALP activity did not appear to change substantially with pristine LDH or the control at all concentrations.

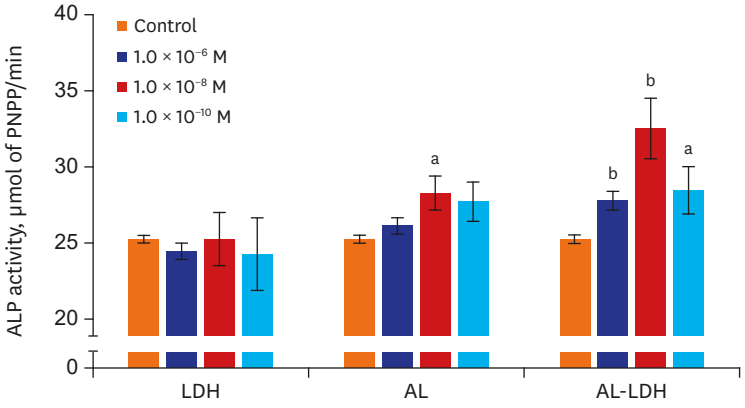

Fig. 7. In vitro ALP activity of MG63 cells treated with osteogenic media containing different concentrations of pristine LDH, intact AL, and AL-LDH for 4 days. For each sample type, at least three experiments were performed for statistics.
ALP = alkaline phosphatase, LDH = layered double hydroxide, AL = alendronate.
[a]Intact AL or AL-LDH was statistically significantly different from both negative control and pristine LDH ($P < 0.05$); [b]AL-LDH was statistically significantly different from the other groups ($P < 0.05$).

https://doi.org/10.3346/jkms.2019.34.e37

When the same dose of AL was applied, both the in vitro cell proliferation and the ALP activity for AL-LDH were more efficiently improved than those for intact AL, which could be ascribed to the facilitated intercellular uptake of AL-LDH; unlike negatively charged AL molecules, the positive zeta potential (0.3 ± 0.15 mV) of AL-LDH nanoparticles led to an enhanced interaction with negatively charged cellular membranes, eventually resulting in favorable cellular uptake based on clathrin-mediated endocytosis.[8,15] Although the pristine LDH itself did not show any effect on the cell proliferation and osteogenic differentiation, the AL intercalated LDH nanohybrid could be considered as a novel drug delivery system (DDS) for improving efficacy of AL.

DISCUSSION

A novel DDS, Al-LDH, was prepared by intercalating AL, one of nitrogen-containing bisphosphonate drug, into LDH nanovehicle. The purpose of this study was not only to suggest the synthetic way of AL-LDH hybrid drug, but to provide the proof of concept, how the LDH delivery vehicle could improve the drug efficacy of AL in terms of the proliferation and osteogenic differentiation on the MG63 cell culture line.

We were successful in establishing the synthetic condition of the hybrid drug, AL-LDH, based on the intercalative ion-exchange reaction, where 2.5-fold excess amount of AL was reacted with the pristine LDH taking into account the AEC of LDH. Since the solution pH could affect on intercalation of AL molecules into LDH due to amphiprotic nature of AL. Thus, we carefully controlled the pH during the reaction based on pKa values of AL (pKa_1, 0.8; pKa_2, 2.2; pKa_3, 6.3; pKa_4, 10.9; and pKa_5, 12.2). According to the PXRD and HR-TEM analyses, the basal spacing of AL-LDH nanohybrid was determined to be 11.3 Å, corresponding to the sum of the layer thickness (4.8 Å) and the van der Waal's diameter (6.5 Å) of AL molecule with parallel orientation. From the in vitro release test, it was found that AL molecules intercalated were rather strongly bound with LDH lattice, and therefore, hardly released out. And the total amount of AL released from Al-LDH was only about to 9.5% after 100 days. According to the cellular uptake studies, the intracellular accumulation of AL in MG63 cells treated with AL-LDH was 10.6-fold higher than that with intact AL for 1 hour treatment. From the CLSM images, the internalization of LDH nanoparticles was confirmed by the localization of green fluorescence within cells due to the intercellular uptake of FITC-LDH-CO_3 itself. Furthermore, in vitro cell proliferation and ALP activity results showed that the incorporation of AL into LDH could enhance efficacy of AL compared to intact AL, although LDH itself had no effect on proliferation and osteogenic differentiation of MG63 cells.

In conclusion, the present AL-LDH could be considered as a promising DDS for improving efficacy of AL.

SUPPLEMENTARY MATERIALS

Supplementary Table 1

Evaluated rate constants and r^2 coefficients based on the kinetic models

Click here to view

https://doi.org/10.3346/jkms.2019.34.e37

Supplementary Fig. 1

Chemical structures and dissociations of AL depending on the values of equilibrium dissociation constant (pKa) of AL. Molar fraction of AL calculated from its pKa values depending on pH.

Click here to view

Supplementary Fig. 2

PXRD patterns of AL intercalated (**A**) $Mg_2Al\_CO_3$ LDH, (**B**) $Mg_2Al\_NO_3$ LDH, and (**C**) $Zn_2Al\_NO_3$ LDH nanohybrids obtained at different reaction times.

Click here to view

Supplementary Fig. 3

(**A**) Chemical structure and (**B**) molecular dimension of AL. (**C**) Schematic diagram of AL molecules intercalated in the LDH layer via intercalative ion-exchange reaction.

Click here to view

Supplementary Fig. 4

(**A-C**) Structural models for the AL-LDH along c-axis. (**D**) The relative X-ray intensity (I_{rel}) of the observed and calculated X-ray intensity of AL-LDH.

Click here to view

Supplementary Fig. 5

(**A**) Absorption spectra of (I) base line ($HClO_4$), (II) AL only, (III) AL-LDH only, (IV) standard Fe^{3+} only, (V-XI) Fe^{3+}–AL complexes with different concentrations of AL, and (XII) Fe^{3+}–AL-LDH complex in 2.0 M $HClO_4$. (**B**) Absorbances of Fe^{3+}–AL complexes depending on the concentration of AL measured at 300 nm using UV-Vis spectroscopy.

Click here to view

Supplementary Fig. 6

Schematic representation of AL-LDH structure. (**A**) The deprotonated phosphate group of AL bound to only one side of LDH layer by strong electrostatic interaction and (**B**) the zipping effect of layered edges bonded with small anions.

Click here to view

Supplementary Fig. 7

The plots of each kinetic equation for the release of AL from the AL-LDH at pH 7.4 PBS media. (**A**) first-order rate model, (**B**) parabolic diffusion model, (**C**) Freundlich model, and (**D**) Elovich model.

Click here to view

Supplementary Fig. 8

PXRD patterns of (**A**) LDH-CO_3 and (**B**) FITC-LDH-CO_3.

Click here to view

https://doi.org/10.3346/jkms.2019.34.e37

Supplementary Fig. 9

FE-SEM images of (**A**) LDH-CO_3 and (**B**) FITC-LDH-CO_3. (**C**) Particle size distributions and (**D**) zeta potentials of LDH-CO_3 (solid line) and FITC-LDH-CO_3 (dashed line), respectively.

Click here to view

Supplementary Fig. 10

Confocal microscopic images of MG63 cells treated with (**A**) 20 μg/mL FITC-LDH-CO_3, (**B**) supernatant solution of 20 μg/mL FITC-LDH-CO_3, and (**C**) 20 μg/mL FITC only.

Click here to view

Supplementary Fig. 11

In vitro proliferation of MG63 cells treated with osteogenic media containing different concentrations of pristine LDH, intact AL, or AL-LDH for (**A**) 2, (**B**) 3, and (**C**) 4 days. All experiments were performed at least three times for statistics.

Click here to view

Supplementary Fig. 12

In vitro ALP activity of MG63 cells treated with osteogenic media containing different concentrations of pristine LDH, intact AL, or AL-LDH for (**A**) 2, (**B**) 3, and (**C**) 4 days. All experiments were performed at least three times for statistics.

Click here to view

REFERENCES

1. Stewart MP, Langer R, Jensen KF. Intracellular delivery by membrane disruption: mechanisms, strategies, and concepts. *Chem Rev* 2018;118(16):7409-531.
PUBMED | CROSSREF
2. Indrigo E, Clavadetscher J, Chankeshwara SV, Megia-Fernandez A, Lilienkampf A, Bradley M. Intracellular delivery of a catalytic organometallic complex. *Chem Commun (Camb)* 2017;53(50):6712-5.
PUBMED | CROSSREF
3. Zhai Y, Ran W, Su J, Lang T, Meng J, Wang G, et al. Traceable bioinspired nanoparticle for the treatment of metastatic breast cancer via NIR-trigged intracellular delivery of methylene blue and cisplatin. *Adv Mater* 2018;30(34):e1802378.
PUBMED | CROSSREF
4. Tan C, Cao X, Wu XJ, He Q, Yang J, Zhang X, et al. Recent advances in ultrathin two-dimensional nanomaterials. *Chem Rev* 2017;117(9):6225-331.
PUBMED | CROSSREF
5. Tan YF, Lao LL, Xiong GM, Venkatraman S. Controlled-release nanotherapeutics: State of translation. *J Control Release* 2018;284:39-48.
PUBMED | CROSSREF
6. Choi G, Jeon IR, Piao H, Choy JH. Highly condensed boron cage cluster anions in 2d carrier and its enhanced antitumor efficiency for boron neutron capture therapy. *Adv Funct Mater* 2018;28(27):1704470.
CROSSREF
7. Kim MH, Hur W, Choi G, Min HS, Choi TH, Choy YB, et al. Theranostic bioabsorbable bone fixation plate with drug-layered double hydroxide nanohybrids. *Adv Healthc Mater* 2016;5(21):2765-75.
PUBMED | CROSSREF

8. Choi G, Piao H, Alothman ZA, Vinu A, Yun CO, Choy JH. Anionic clay as the drug delivery vehicle: tumor targeting function of layered double hydroxide-methotrexate nanohybrid in C33A orthotopic cervical cancer model. *Int J Nanomedicine* 2016;11:337-48.
PUBMED | CROSSREF
9. Choi G, Kim TH, Oh JM, Choy JH. Emerging nanomaterials with advanced drug delivery functions. focused on methotrexate delivery. *Coord Chem Rev* 2018;359:32-51.
CROSSREF
10. Oh JM, Park DH, Choi SJ, Choy JH. LDH nanocontainers as bio-reservoirs and drug delivery carriers. *Recent Pat Nanotechnol* 2012;6(3):200-17.
PUBMED | CROSSREF
11. Lee SS, Choi GE, Lee HJ, Kim Y, Choy JH, Jeong B. Layered double hydroxide and polypeptide thermogel nanocomposite system for chondrogenic differentiation of stem cells. *ACS Appl Mater Interfaces* 2017;9(49):42668-75.
PUBMED | CROSSREF
12. Choy JH, Kwak SY, Jeong YJ, Park JS. Inorganic layered double hydroxides as nonviral vectors. *Angew Chem Int Ed Engl* 2000;39(22):4041-5.
PUBMED | CROSSREF
13. Choi G, Eom S, Vinu A, Choy JH. 2D nanostructured metal hydroxides with gene delivery and theranostic functions; a comprehensive review. *Chem Rec* 2018;18(7-8):1033-53.
PUBMED | CROSSREF
14. Li S, Li J, Wang C, Wang Q, Cader MZ, Lu J, et al. Cellular uptake and gene delivery using layered double hydroxide nanoparticles. *J Mater Chem B Mater Biol Med* 2013;1(1):61-8.
CROSSREF
15. Oh JM, Choi SJ, Kim ST, Choy JH. Cellular uptake mechanism of an inorganic nanovehicle and its drug conjugates: Enhanced efficacy due to clathrin-mediated endocytosis. *Bioconjug Chem* 2006;17(6):1411-7.
PUBMED | CROSSREF
16. Gu Z, Zuo HL, Li L, Wu AH, Xu ZP. Pre-coating layered double hydroxide nanoparticles with albumin to improve colloidal stability and cellular uptake. *J Mater Chem B Mater Biol Med* 2015;3(16):3331-9.
CROSSREF
17. Choi SJ, Choy JH. Layered double hydroxide nanoparticles as target-specific delivery carriers: uptake mechanism and toxicity. *Nanomedicine (Lond)* 2011;6(5):803-14.
PUBMED | CROSSREF
18. Lv F, Xu L, Zhang Y, Meng Z. Layered double hydroxide assemblies with controllable drug loading capacity and release behavior as well as stabilized layer-by-layer polymer multilayers. *ACS Appl Mater Interfaces* 2015;7(34):19104-11.
PUBMED | CROSSREF
19. Choi G, Lee JH, Oh YJ, Choy YB, Park MC, Chang HC, et al. Inorganic-polymer nanohybrid carrier for delivery of a poorly-soluble drug, ursodeoxycholic acid. *Int J Pharm* 2010;402(1-2):117-22.
PUBMED | CROSSREF
20. Kajiwara H, Yamaza T, Yoshinari M, Goto T, Iyama S, Atsuta I, et al. The bisphosphonate pamidronate on the surface of titanium stimulates bone formation around tibial implants in rats. *Biomaterials* 2005;26(6):581-7.
PUBMED | CROSSREF
21. Rodan GA, Martin TJ. Therapeutic approaches to bone diseases. *Science* 2000;289(5484):1508-14.
PUBMED | CROSSREF
22. Bukowski JF, Dascher CC, Das H. Alternative bisphosphonate targets and mechanisms of action. *Biochem Biophys Res Commun* 2005;328(3):746-50.
PUBMED | CROSSREF
23. Xiong Y, Yang HJ, Feng J, Shi ZL, Wu LD. Effects of alendronate on the proliferation and osteogenic differentiation of MG-63 cells. *J Int Med Res* 2009;37(2):407-16.
PUBMED | CROSSREF
24. Reinholz GG, Getz B, Pederson L, Sanders ES, Subramaniam M, Ingle JN, et al. Bisphosphonates directly regulate cell proliferation, differentiation, and gene expression in human osteoblasts. *Cancer Res* 2000;60(21):6001-7.
PUBMED
25. von Knoch F, Jaquiery C, Kowalsky M, Schaeren S, Alabre C, Martin I, et al. Effects of bisphosphonates on proliferation and osteoblast differentiation of human bone marrow stromal cells. *Biomaterials* 2005;26(34):6941-9.
PUBMED | CROSSREF

26. Fazil M, Baboota S, Sahni JK, Ameeduzzafar , Ali J. Bisphosphonates: therapeutics potential and recent advances in drug delivery. *Drug Deliv* 2015;22(1):1-9.
PUBMED | CROSSREF

27. Chakraborti M, Jackson JK, Plackett D, Brunette DM, Burt HM. Drug intercalation in layered double hydroxide clay: application in the development of a nanocomposite film for guided tissue regeneration. *Int J Pharm* 2011;416(1):305-13.
PUBMED

28. Kuljanin J, Janković I, Nedeljković J, Prstojević D, Marinković V. Spectrophotometric determination of alendronate in pharmaceutical formulations via complex formation with Fe(III) ions. *J Pharm Biomed Anal* 2002;28(6):1215-20.
PUBMED | CROSSREF

29. Itano N, Atsumi F, Sawai T, Yamada Y, Miyaishi O, Senga T, et al. Abnormal accumulation of hyaluronan matrix diminishes contact inhibition of cell growth and promotes cell migration. *Proc Natl Acad Sci U S A* 2002;99(6):3609-14.
PUBMED | CROSSREF

30. Park DH, Yang JH, Vinu A, Elzatahry A, Choy JH. X-ray diffraction and X-ray absorption spectroscopic analyses for intercalative nanohybrids with low crystallinity. *Arab J Chem* 2016;9(2):190-205.
CROSSREF

31. Benyettou F, Chebbi I, Motte L, Seksek O. Magnetoliposome for alendronate delivery. *J Mater Chem* 2011;21(13):4813-20.
CROSSREF

32. Liu X, Qu S, Lu X, Ge X, Leng Y. Time-of-flight secondary ion mass spectrometry study on the distribution of alendronate sodium in drug-loaded ultra-high molecular weight polyethylene. *Biomed Mater* 2009;4(6):065008.
PUBMED | CROSSREF

33. Errassifi F, Sarda S, Barroug A, Legrouri A, Sfihi H, Rey C. Infrared, Raman and NMR investigations of risedronate adsorption on nanocrystalline apatites. *J Colloid Interface Sci* 2014;420:101-11.
PUBMED | CROSSREF

34. Yang JH, Han YS, Park M, Park T, Hwang SJ, Choy JH. New inorganic-based drug delivery system of indole-3-acetic acid-layered metal hydroxide nanohybrids with controlled release rate. *Chem Mater* 2007;19(10):2679-85.
CROSSREF

35. Choi SJ, Choy JH. Effect of physico-chemical parameters on the toxicity of inorganic nanoparticles. *J Mater Chem* 2011;21(15):5547-54.
CROSSREF

36. Choi SJ, Oh JM, Choy JH. Biocompatible ceramic nanocarrier for drug delivery with high efficiency. *J Ceram Soc Jpn* 2009;117(1365):543-9.
CROSSREF